Steady-state erosion of propagating ion beams

D. V. Rose,[a] T. C. Genoni, and D. R. Welch
Mission Research Corporation, Albuquerque, New Mexico 87110

(Received 19 September 2001; accepted 20 December 2001)

A steady-state analytic model of beam erosion is presented and compared with two-dimensional hybrid particle-in-cell simulations of 100 MeV to 2 GeV proton beams propagating in a dense background gas. The analytic model accounts for nonzero beam erosion front velocities and the finite energies of beam particles radially exiting the beam through a single parameter. The model is in agreement with the simulation results for a single value of this parameter over the beam energy ranges considered. © *2002 American Institute of Physics.* [DOI: 10.1063/1.1452102]

A charged particle beam propagating in a gas is neutralized only after the gas begins to be ionized. The unneutralized beam head expands at a rate governed by the net Lorentz force and the beam divergence. Behind the beam head, the rising conductivity neutralizes the beam space charge and the net azimuthal magnetic field acts as a pinch force, which can confine the beam divergence if this force is large enough. The net azimuthal magnetic field is the difference of the beam magnetic field and the magnetic field of the plasma return current. In addition, an axial electric field is induced in the beam, arising from the finite conductivity of the plasma and subsequent decay of the plasma currents. This electric field acts to slow the beam particles, resulting in a net energy loss to the beam.

Previous work (see, for example, Refs. 1–4) has primarily examined the erosion of self-pinched relativistic electron beams in gas and plasma (including ion-focused-regime propagation). Numerical simulations (see, for example, Refs. 5 and 6) have also examined various electron beam erosion processes, and several experiments have examined the erosion of electron beam pulses in preformed plasmas.[7,8] In this paper, we examine the erosion of intense ion beams propagating in a dense gas. The scalar conductivity model available in the IPROP hybrid particle-in-cell code[9] is used which is valid for high gas pressures where significant net currents are expected (due to recombination). We expect the analytic model presented below to be independent of the processes that lead to net current generation, making this work applicable to a variety of other beam transport problems. These applications include transport of intense light-ion beams for inertial-confinement-fusion (ICF),[10,11] a proposed scheme for long-distance propagation ($\gtrsim$100 m) of heavy ion beams from an accelerator to a reactor chamber as well as transport inside of the reactor chamber for heavy-ion ICF (HIF).[12]

We consider a steady state model of an ion beam of current I_b and energy $(\gamma-1)Am_pc^2$ being continuously injected into a box fixed in the laboratory frame as in Fig. 1. Here, γ is the relativistic mass factor, m_p is the proton mass, A is the atomic number, and c is the speed of light. The head of the beam moves with the front velocity $\beta_F c$. The rate at which particles are being injected is I_b/Ze, where e is the magnitude of the electron charge and Z is the beam ion charge state. In a time interval Δt a length of beam $\beta_F c\Delta t$ will be added to the tail of the beam, so that the rate at which the number of particles in the box is increasing is

$$\beta_F c n_b \pi R^2 = \frac{\beta_F}{\beta}\frac{I_b}{Ze}, \tag{1}$$

and it follows that beam ions must be leaving the box at a rate $(1-\beta_F/\beta)I_b/Ze$. In Eq. (1), R is the beam radius and n_b is the beam number density. The rate of increase of magnetic field energy within the box is just

$$\beta_F c\int_0^{R_w}\frac{B_\theta^2}{8\pi}2\pi r\,dr = \beta_F c\frac{I_n^2 L}{c^2}, \tag{2}$$

where I_n is the net current and L is a dimensionless inductance, the leading term of which is $\ln(R_w/R)$ for a $1/r$ azimuthal magnetic field profile. R_w is the radius at which $B_\theta \rightarrow 0$. Here L is determined from Eq. (2) by integrating over $B_\theta(r)$ obtained from the simulation results and found to be of order 4.

Balancing the *net* inflow of particle kinetic energy with the rate of increase of kinetic plus magnetic field energy within the box leads to

$$(\gamma-1)Am_pc^2\frac{I_b}{Ze}-\alpha(\gamma_F-1)Am_pc^2\left(1-\frac{\beta_F}{\beta}\right)\frac{I_b}{Ze} = \frac{\beta_F}{\beta}(\gamma-1)Am_pc^2\frac{I_b}{Ze}+\beta_F\frac{I_n^2}{c}L, \tag{3}$$

where the parameter α specifies the fraction of the ''front kinetic energy'' the exiting particles carry away. For the case of a semi-infinite beam where the plasma currents have decayed to zero in the tail, $I_n \rightarrow I_b$ in Eq. (3). Combining terms and simplifying gives

$$\left(1-\frac{\beta_F}{\beta}\right) = \frac{\beta_F X}{(\gamma-1)-\alpha(\gamma_F-1)}, \tag{4}$$

where

$$X \equiv \frac{I_n^2(\mathrm{kA})L}{17MI_b(\mathrm{kA})}, \tag{5}$$

[a]Electronic mail: drose@mrcabq.com

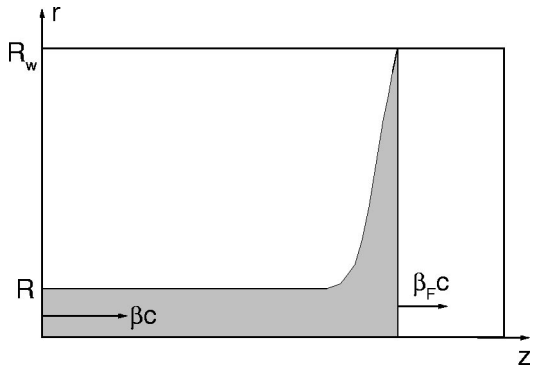

FIG. 1. Schematic of the steady state beam model. Beam particles are injected into the box from the left with a speed βc and the beam head propagates forward with a speed $\beta_F c$, where $\beta_F < \beta$.

$M = Am_p/Zm_e$, and $(1-\beta_F/\beta)$ is the dimensionless erosion rate. Making the substitution $\gamma_F = 1/\sqrt{1-\beta_F^2}$ in Eq. (4) gives an equation which can be solved numerically for the single unknown β_F, and hence the erosion rate.

Using $\alpha = 1$ in Eq. (4) describes the case where the beam particles leave the box with the kinetic energy associated with the front velocity. This produces results that are within a factor of 2 of those calculated from the formula derived by Mostrom *et al.*[3] using a flux conservation argument. It also agrees very closely with the calculations of Sharp *et al.*[1] for relativistic electron beams (taking $M = 1$).

For comparison with the simulations presented below, we consider herein the specific case of proton beams ($M = 1836$) with $I_b = 10$ kA, $I_n = 5$ kA, and $L = 4$. Figure 2 plots the dimensionless erosion rate for different values of α as a function of the injected beam particle energy, E_b. Using $\alpha = 1$ in Eq. (4) produces the upper curve in Fig. 2. Equation (4) with $\alpha = 0$ has also been used as an erosion rate estimate[13] and produces the lower curve in Fig. 2.

The particle-in-cell code IPROP[9] is used with a model for tracking the evolution of the background gas conductivity and plasma currents. These two-dimensional (r,z) simulations use the IPROP implicit field solver. The beam is injected into a 600 cm long simulation region. The beam propagates into the stationary mesh until the beam head is

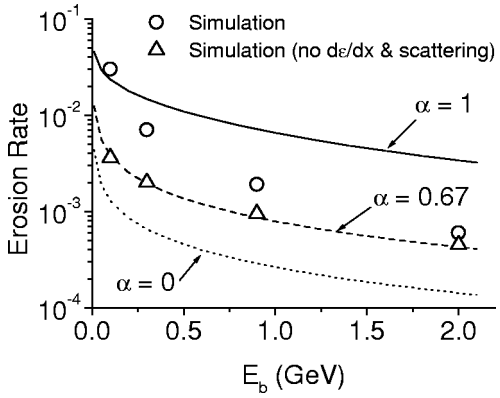

FIG. 2. The dimensionless erosion rate $(1-\beta_F/\beta)$ as a function of injected proton beam energy. The curves are calculated from Eq. (4) and the data points are from IPROP simulations.

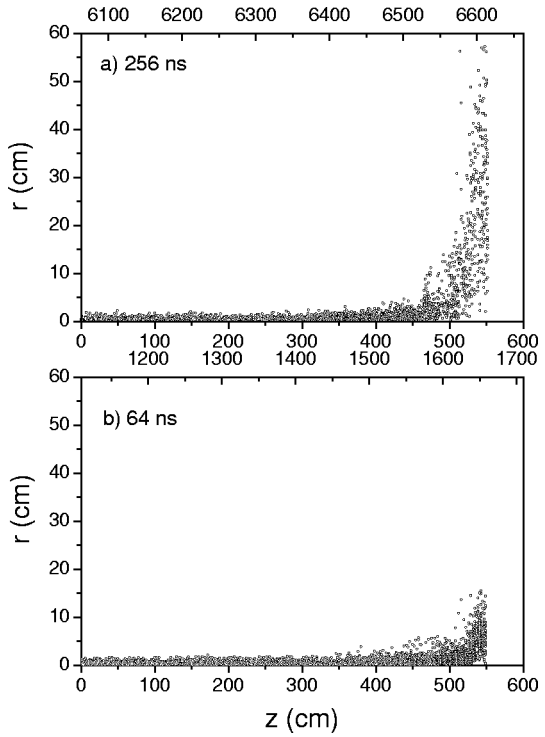

FIG. 3. Beam particle positions at (a) 256 ns and (b) 64 ns. The lower axis of each plot shows beam frame axial position and the upper axis show the laboratory frame axial coordinate.

within 50 cm of the downstream boundary. At this time, the mesh is moved forward at the injected beam speed. The beam energy is tracked as the beam passes through diagnostic planes located 600 cm apart (in the laboratory frame). The time-integrated beam energy from these diagnostics is used to determine the total dimensionless erosion rate of the beam. The injected beam ($M = 1836$) has a 1 cm radius Bennett current-density profile, $J_b(r) \propto (1+(r/R)^2)^{-2}$. The beam current rises linearly from zero to a peak current of 10 kA over 150 cm. The injected beam is monoenergetic (with a single particle energy E_b), and is injected with a transverse momentum spread that provides a near optimal matching condition for injection into 760 torr N_2. Simulations with and without $d\epsilon/dx$ mass stopping and scattering[14] of the beam ions were carried out as part of this investigation. The simulations that do not include $d\epsilon/dx$ mass stopping and scattering provide more direct comparisons with the model.

Insight into the physics of the inductive erosion process is provided by Figs. 3–5 which summarize the results of a simulation with $E_b = 900$ MeV. This simulation does not include $d\epsilon/dx$ mass stopping and scattering of the beam. In Fig. 3, the beam particle positions are shown at 64 ns and 256 ns. The upper horizontal axis on each plot in Fig. 3 is the laboratory z coordinate while the lower horizontal axis is the beam-frame z coordinate. At 256 ns [Fig. 3(a)], the beam head has expanded out to the radial wall at $r = 60$ cm, while the beam body remains in a self-pinched equilibrium.

The axial momentum of the beam, shown in Fig. 4, demonstrates the effect of the inductive axial electric field on the beam. The lower frame [Fig. 4(b)] shows the beam particles at 64 ns. The axial injection momentum is about 1.68 in units

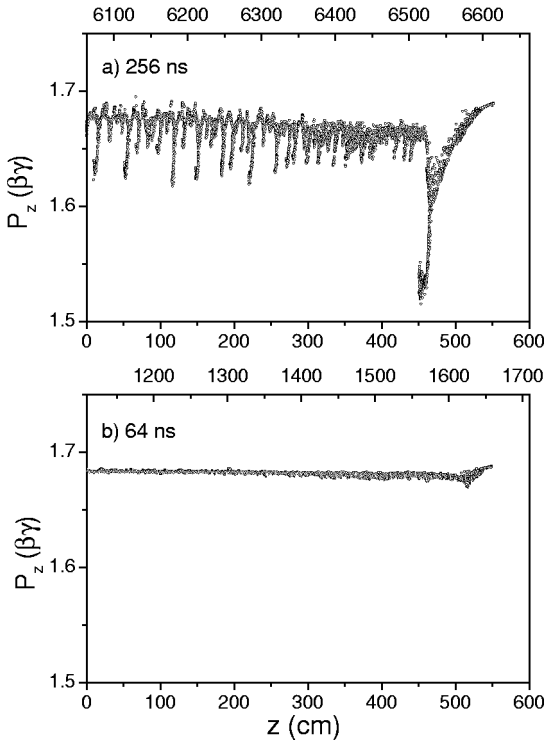

FIG. 4. Beam particle phase space at (a) 256 ns and (b) 64 ns. The lower axis of each plot shows beam frame axial position and the upper axis show the laboratory frame axial coordinate.

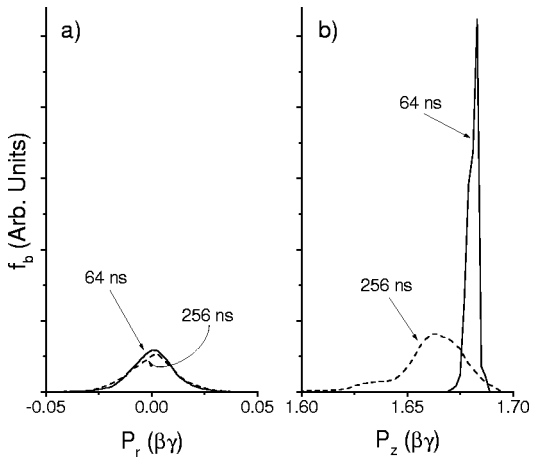

FIG. 5. Radial (a) and axial (b) momentum distributions for the beam at 64 ns (solid lines) and 256 ns (dashed lines).

of $\beta\gamma$ ($\sim$900 MeV). The slight decrease in P_z along the beam length is due to slowing by the inductive electric field. After 256 ns [Fig. 4(a)], a large drop in the axial momentum is observed near the beam head, where the beam ''trumpet'' has formed (extending to the outer wall of the simulation at $r=60$ cm). Also many smaller spikes in P_z develop along the beam, increasing in amplitude from the beam head to tail. These spikes, which are correlated with E_z field spikes along the beam length, are of smaller amplitude than the large E_z spike near the beam head. This electric field structure has also been observed in other numerical simulations, particularly in ion-focused channel transport for relativistic electron beams,[5] where the channel density is greater than the beam density. In the present simulations, the spikes form due to the finite resistivity of the plasma.

The hook-like feature that develops near the beam head in Fig. 4(a) is a result of the original, low-current beam head particles falling back and becoming trapped in the new evolving beam head. Although not shown, simulations that include $d\epsilon/dx$ mass stopping and scattering of the beam develop a similar phase-space character, including the ''hook-like'' feature in the axial momentum near the beam head.

Compared with the change in the observed axial momentum spread, the change in the average radial momentum spread is very small over these times scales. Figure 5 shows the radial (a) and axial (b) momentum distribution functions (f_b) for the beam at 64 ns and 256 ns. The spread in the radial momentum distribution shown in Fig. 5(a) does increase slightly between 64 ns and 256 ns, while the average axial momentum shown in Fig. 5(b) is significantly reduced over this same time interval. The axial momentum spread becomes approximately equal to the radial momentum spread on these time scales.

It is apparent from the simulation results that particles leave the beam with a range of energies up to and including the erosion front energy γ_F, although a rigorous determination of α from the simulation diagnostics has not been attempted. For the comparisons with the model in Fig. 2, the α parameter that empirically provides the best fit to the simulations that do not include $d\epsilon/dx$ mass stopping and scattering of the beam is 0.67. Particles with radii greater than $\sim 3R$ are not trapped within the beam and eventually strike the radial boundary of the simulation box, where they are absorbed. These particles have a range of energies as they escape the beam body, but they are accelerated by the net radial electric field in the vicinity of the beam head.

The erosion rate for the simulations that include $d\epsilon/dx$ mass stopping and scattering of the beam do not fit on a constant α curve, because $d\epsilon/dx$ mass stopping decreases for proton energies between 100 MeV and 2 GeV.[15] An average dimensionless $d\epsilon/dx$ erosion rate can be calculated and added to the inductive erosion rate obtained above (using $\alpha = 0.67$). This combined erosion rate, shown in Fig. 6, is in good agreement with the simulations that include $d\epsilon/dx$ mass stopping and scattering of the beam.

A model of the steady-state erosion of intense ion beams in a background gas is presented and found to be in good agreement with detailed two-dimensional hybrid particle-in-cell simulations for injected proton beam energies between 100 MeV and 2 GeV. The model uses a free parameter, α, that enables comparison with other models as well as comparison with the simulations. Using $\alpha \simeq 0.67$ in Eq. (4) gives reasonable agreement with the simulations that do not include $d\epsilon/dx$ mass stopping and scattering of the ion beam. Adding a $d\epsilon/dx$ mass stopping erosion rate to this result gives a total erosion rate that is in agreement with the simulations that include beam ion stopping and scattering.

Here the model is compared with simulations of proton beams propagating in high pressure (760 torr N_2) gas, where the IPROP scalar conductivity model is valid and significant

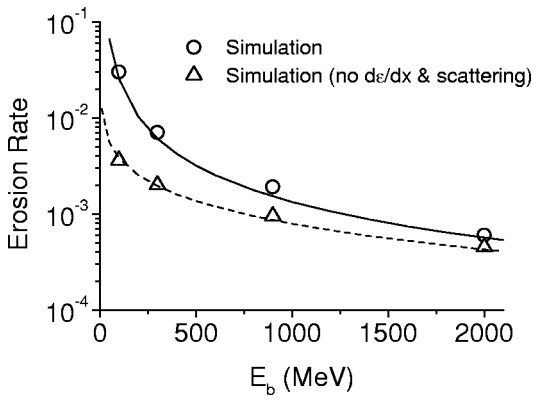

FIG. 6. The dimensionless erosion rates as a function of injected proton beam energy. The dashed curve is calculated from Eq. (4) with $\alpha=0.67$ and the solid curve adds this result to a calculated $d\epsilon/dx$ dimensionless erosion rate. The data points are from IPROP simulations.

net currents develop. Work is presently underway to compare the model with erosion rates from more stressing simulations of heavy ion beams propagating in lower pressure background gases with densities on order of the beam density.[16] For example, sample HIF beam parameters for self-pinched propagation ($E_b=2.4$ GeV Xe^{+65}, $I_b=65$ kA, $I_n=10$ kA) give a dimensionless erosion rate of ~ 0.003 for $\alpha=0.67$ and $L=4$. For reactor chamber propagation distances of ~ 5 m, beam erosion is negligible (~ 1.5 cm), but for the final drift section outside of the chamber (~ 100 m),[12] a significant portion of a self-pinch propagated beam would be eroded.

ACKNOWLEDGMENTS

The authors gratefully acknowledge discussions with Dr. C. L. Olson and Dr. M. G. Mazarakis.

This work was supported by U.S. Department of Energy through Sandia National Laboratories.

[1] W. M. Sharp and M. Lampe, Phys. Fluids **23**, 2383 (1980).
[2] H. L. Buchanan, Phys. Fluids **30**, 221 (1987).
[3] M. A. Mostrom, D. Mitrovich, D. R. Welch, and M. M. Campbell, Phys. Plasmas **3**, 3469 (1996).
[4] E. P. Lee, Lawrence Berkeley National Laboratory, private communication, 2001.
[5] J. Krall, K. Nguyen, and G. Joyce, Phys. Fluids B **1**, 2099 (1989).
[6] L. V. Glazychev and G. A. Sorokin, Sov. J. Plasma Phys. **16**, 210 (1990).
[7] L. Y. Chan and R. L. Stenzel, Phys. Rev. Lett. **67**, 2147 (1991).
[8] P. W. Werner, E. Schamiloglu, J. R. Smith, K. W. Struve, and R. J. Lipinski, Phys. Rev. Lett. **73**, 2986 (1994).
[9] D. R. Welch, C. L. Olson, and T. W. L. Sanford, Phys. Plasmas **1**, 764 (1994).
[10] P. F. Ottinger, D. V. Rose, and C. L. Olson, J. Appl. Phys. **75**, 4402 (1994).
[11] D. R. Welch, M. E. Cuneo, C. L. Olson, and T. A. Mehlhorn, Phys. Plasmas **3**, 2113 (1996).
[12] K. Hahn and E. Lee, Fusion Eng. Des. **32–33**, 417 (1996).
[13] C. L. Olson, Sandia National Laboratories, private communication, 1999.
[14] See, for example, J. D. Jackson, *Classical Electrodynamics*, 2nd ed. (Wiley, New York, 1975), p. 641.
[15] See, for example, A. M. Hillas, *Cosmic Rays* (Pergamon, Oxford, 1972), p. 30.
[16] P. F. Ottinger, F. C. Young, S. J. Stephanakis *et al.*, Phys. Plasmas **7**, 346 (2000).